Extraction of differential cross sections by the method of moments. I. Photodissociation

G. Bandukwalla and M. F. Vernon

Extraction of differential cross sections by the method of moments. I. Photodissociation

G. Bandukwalla
Department of Physics, Columbia University, New York, New York 10027

M. F. Vernon[a)]
Department of Chemistry, Columbia University, New York, New York 10027

We describe a general way of extracting the center-of-mass frame differential photodissociation cross section from the space-fixed fragment time-of-flight distributions obtained in laboratory experiments. Our approach is a variant of the method of moments and involves only elementary numerical computations. Experimental resolution and error analysis are naturally incorporated in the methodology. Several numerical examples are provided for the purpose of illustration.

I. INTRODUCTION

In a wide variety of molecular beam experiments one is faced with extracting the center-of-mass frame differential cross section for a scattering process from the measured time-of-flight data of the scattered particles. For instance, in crossed laser-molecular beam experiments the photoproducts are created in a localized volume (the interaction region) and travel a nominally fixed length (the flight path) to a particle detector here taken to be a mass spectrometer. When pulsed lasers ($\sim$10–20 ns) are used to initiate the photodissociation, and if the flight path is sufficiently long, then the time evolution of the signal at the detector (the time-of-flight spectra) will be a clear, direct measurement of the photofragment velocity distribution. Often, kinematic or experimental practicalities prohibit a direct translation of the measured TOF spectra obtained in the space-fixed laboratory reference frame to the more fundamental center-of-mass frame product velocity distribution. However, since the conditions of the scattering experiment are known or determinable, it is desirable to use as much of this information as possible to remove the known systematic averaging from the experimental measurements in the last biased manner.

For photofragmentation, the center-of-mass differential cross section for scattering into a solid angle $d\Omega$ with translational energy E (hereafter abbreviated as DFCS) can be written in the electric dipole approximation as

$$\frac{d^2\sigma}{d\Omega\, dE} = P(E,\Theta) = P(E)\left[1 + \beta P_2(\cos\Theta)\right], \qquad (1)$$

where β is the anisotropy parameter, $P_2(\cos\Theta)$ is the second Legendre polynomial of $\cos\Theta$, and Θ is the angle between the center-of-mass fragment recoil velocity and laser polarization vector. Bersohn and others[1] have shown that β depends on the angle between the electronic transition moment and the bond dissociation axis as well as the time scale for the photodissociation process. The product translational energy distribution $P(E)$ does not have a strict functional form and is highly dependent on the dynamics and the potential energy surfaces governing the photodissociation process.

In an ideal experiment, the interaction and detection regions are taken to be differential volume elements and the speed distribution of the molecular beam a delta function centered at the flow velocity. The integrated scattered signal for a differentially small time interval delayed by an amount t_i from the firing of the laser will require knowing the DFCS only at the point (E_i,Θ_i) whose exact value can be seen geometrically in Fig. 1. In practice, the interaction and detection regions are not differentially small, the initial molecular beam speed distribution is not a delta function, and the signal is electronically integrated over a finite time interval so the experimentally measured scattered signal at a nominal time delay t_i will sample the DFCS over a finite range of (E,Θ).

The problem is to then find an extraction procedure which gives a best value for the anisotropy β and the translational energy function $P(E)$ while accounting for the measured initial velocity distribution of the particle velocities before dissociation and for the known finite dimensions of the interaction and detection regions. In this paper we present a variant of the method of moments[2] which can be used for extracting the photodissociation DFCS from the experimental TOF scattering data. The method is computationally
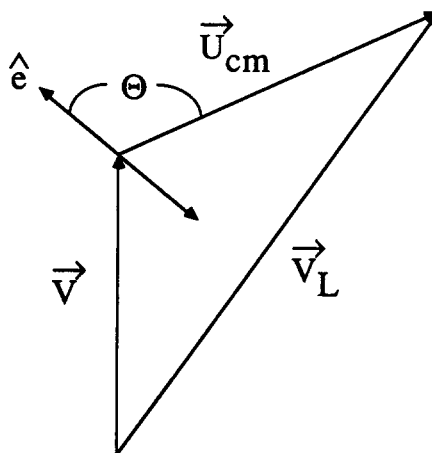

FIG. 1. Velocity vector diagram showing the geometrical relationship between the molecular beam velocity **v**, the center-of-mass recoil velocity of the photofragment $\mathbf{u}_{c.m.}$, the laboratory of the photofragment $\mathbf{v}_L$, the laser polarization axis **e**, and the angle between the laser polarization vector and center-of-mass velocity vector Θ.

efficient and satisfies our criteria for an unbiased procedure with rigorous error estimates which can be applied directly to experimental data.

The organization of this paper is as follows. We begin with an outline of the method, followed by the definition of the "linear approximation" which is the simplest and most fundamental application. We subsequently modify the linear approximation to deal with the standard case of photodissociation in the dipole approximation [Eq. (1)] and show how to obtain both the translational energy distribution $P(E)$ and anisotropy parameter β. We then extend the methodology to include higher order corrections, the first which we call the "quadratic approximation." Finally we consider several examples which illustrate the theory for realistic conditions and comment on the limitations of the method.

II. THEORY OF THE METHOD OF MOMENTS

Let Δt be the width of the time interval (or bin) used to resolve the arrival time dependence of the scattered fragments at the detector. For each detector angle setting Ω_{lab}, the number of counts accumulated for the ith time bin will be

$$R_i = R(t_i, \Omega_{lab})$$

$$= C \int dt \int d\mathbf{r} \int d\mathbf{R} \int dv \, W(v) J(t, \mathbf{r}, \mathbf{R}, v) P(E, \Theta) , \quad (2)$$

where $W(v)$ is the speed distribution of the molecular beam, $J(t, \mathbf{r}, \mathbf{R}, v)$ the Jacobian for the transformation from the center-of-mass frame to the laboratory reference frame, and C is an overall normalization constant involving the detection efficiency, photon and molecular beam fluxes. It is understood that E and Θ are generally complicated but given functions of the variables t, $\mathbf{r}$, $\mathbf{R}$, and v. Explicit expressions for the quantities which appear in the integrand in terms of the integration variables are given in the Appendix. We follow the convention that a non-boldface vector variable is the length of the vector.

The key to our method is the observation that the R_i can be formally expanded as a Taylor series in the variables E and Θ about their average values (E_i, Θ_i) for the ith time bin

$$P(E, \Theta) = P(E_i, \Theta_i) + \frac{dP}{dE} (E - E_i)$$

$$+ \frac{dP}{d\Theta} (\Theta - \Theta_i) + \cdots . \quad (3)$$

This expansion will be useful if the domain of E and Θ probed is sufficiently small such that a truncated Taylor series forms a good approximation to the DFCS for the ith time interval.

To illustrate the method, we consider first the linear approximation which retains terms of the Taylor series through the first derivatives. We introduce the notation

$$\langle X \rangle_i = C \int dt \int d\mathbf{r} \int d\mathbf{R} \int dv \, W(v) J(t, \mathbf{r}, \mathbf{R}, v) X \quad (4)$$

in terms of which

$$E_i = \frac{\langle E \rangle_i}{\langle 1 \rangle_i} \quad (5)$$

and

$$\Theta_i = \frac{\langle \Theta \rangle_i}{\langle 1 \rangle_i} . \quad (6)$$

Using the linear approximation for the right-hand side of Eq. (2) we have

$$R_i = \langle P(E, \Theta) \rangle_i = P(E_i, \Theta_i) \langle 1 \rangle_i$$

$$+ \frac{dP}{dE} \langle E - E_i \rangle_i + \frac{dP}{d\Theta} \langle \Theta - \Theta_i \rangle_i . \quad (7)$$

Dividing Eq. (7) by the volume element $\langle 1 \rangle_i$ gives

$$\frac{R_i}{\langle 1 \rangle_i} = P(E_i, \Theta_i)$$

$$+ \frac{dP}{dE} \left(\frac{\langle E \rangle_i}{\langle 1 \rangle_i} - E_i \right) + \frac{dP}{d\Theta} \left(\frac{\langle \Theta \rangle_i}{\langle 1 \rangle_i} - \Theta_i \right)$$

$$= P(E_i, \Theta_i) . \quad (8)$$

For each R_i we obtain in the linear approximation a value for the DFCS at the point (E_i, Θ_i) given simply by

$$P(E_i, \Theta_i) = \frac{R_i}{\langle 1 \rangle_i} . \quad (9)$$

Hence, the collection $\{R_i\}$ for the different time intervals and laboratory detector angles gives a set of values for the DFCS at discrete points in the E–Θ plane. It is important to note that the set of points $\{E_i, \Theta_i\}$ in the energy-angle variables are provided and determined by the method itself, rather than being subject to some arbitrary choice at the outset. Furthermore, statistical and systematic error analysis can immediately be performed. Namely, let ΔR_i denote the absolute experimental error in R_i. It follows trivially from Eq. (9) that the error in the DFCS is

$$\Delta P(E_i, \Theta_i) = \frac{\Delta R_i}{\langle 1 \rangle_i} \quad (10)$$

provided the error computed by Eq. (10) is larger than the error due to the application of the linear approximation itself. The error of the linear approximation is discussed in detail below.

A. Linear approximation: Anisotropic case

In the case of photofragmentation the DFCS has the reduced form of Eq. (1). The known analytical form of the angular dependence can be exploited to obtain a better approximation scheme for determining the anisotropy parameter β. In the linear approximation, if the anisotropy parameter β were already known, the product energy distribution would be given by

$$P(E_i) = \frac{R_i}{\langle 1 \rangle_i [1 + \beta P_2(\cos \Theta_i)]} . \quad (11)$$

Note that Eq. (11) "corrects" each experimental count rate R_i for the angular anisotropy by evaluating the second Legendre factor at the average value of Θ appropriate for that time bin. It is clear that if the average value of the second Legendre polynomial itself was used in Eq. (11), then all orders of the angular dependence in Eq. (3) can be accounted for exactly. To do this, the angular dependence is ab-

sorbed into the definition of the expectation brackets of Eq. (4). Now the analogous expansion scheme for Eq. (9) becomes

$$\frac{R_i}{\langle\langle 1 \rangle\rangle_i} = P(E_i) , \qquad (12)$$

where the expectations are explicitly dependent on β through

$$1(\beta) = \langle\langle 1 \rangle\rangle_i , \qquad (13)$$

$$E_i(\beta) = \frac{\langle\langle E \rangle\rangle_i}{\langle\langle 1 \rangle\rangle_i} , \qquad (14)$$

where the new definition of the expectation brackets is

$$\langle\langle X \rangle\rangle_i = C \int dt \int d\mathbf{r} \int d\mathbf{R}$$

$$\times \int dv \, W(v) J(t,\mathbf{r},\mathbf{R},v) [1 + \beta P_2(\cos\Theta)] X . \qquad (15)$$

To determine the anisotropy parameter β we work backward from Eq. (12) by a self-consistent method. If an incorrect value of β were used in Eq. (12), then the derived $\{P(E_i)\}$ points will not fall along a universal $P(E)$ curve within the experimental error limits because the true anisotropy correction factor has not been applied to each data point. We define a nonparametric measure of the deviation from the true $P(E)$ curve, $B(\beta)$, as

$$B(\beta) = \frac{\Sigma [P(E_{i-1}) - P(E_i)]^2}{[\Sigma P(E_i)]^2} . \qquad (16)$$

The numerator is simply the sum of the squares of the difference of adjacent translational energy points where it is assumed that the E_i are ordered by size, i.e., $E_1 < E_2 < E_3 \cdots$. The denominator insures that $B(\beta)$ is dimensionless and therefore independent of any overall constant multiplicative factor of either R_i or $\langle\langle 1 \rangle\rangle_i$. The best choice for β can be found by minimizing the expression for $B(\beta)$ *providing* that for any data point E_i there are many nearby data points with nearly the same energy but with different angular averaging.

B. Quadratic approximation: Isotropic case

If the experimental parameters are chosen in such a way that the previously discussed linear approximation gives accurate information on the DFCS, then one is fundamentally

limited only by the statistical errors in the TOF data, $\{R_i\}$. It is important to know how in principle one can proceed beyond the linear approximation in order to improve the results and/or provide criteria for accuracy when either the DFCS is rapidly changing or the experimental averaging is significant. For the purpose of illustrating how the accuracy of the method can be improved we consider the isotropic case ($\beta = 0$) where the second derivative term in Eq. (3) is included. The TOF data are now given by

$$\frac{R_i}{\langle 1 \rangle_i} = P(E_i) + [E_i^2 - (E_i)^2] \frac{P''(E_i)}{2} , \qquad (17)$$

where

$$E_i^2 = \frac{\langle E^2 \rangle_i}{\langle 1 \rangle_i} \qquad (18)$$

and $P''(E_i)$ is the second derivative of the translational energy distribution at E_i.

Equation (17) shows that the neglected terms in the Taylor series are important if the combined effect of a rapidly varying translational energy distribution [in which case the derivatives $P''(E_i), P''(E_i),\ldots$ are large] or the experimental averaging of the scattering kinematics is significant (the dispersion and higher order moments of the translational energy distribution for the time bins are large) and results in a Taylor series expansion which is not converged to the desired accuracy by using only the linear approximation.

III. EXAMPLES

Before we apply our method to experimental data, we want to explore the reliability and convergence properties with a few well defined test cases. We proceed by assuming an explicit functional form for $P(E,\Theta)$ and compute the exact set of $\{R_i\}$ which a noise free experiment would measure for this assumed $P(E,\Theta)$. We consider these $\{R_i\}$ as data from an experiment which we analyze by the method of moments to recover an estimate of $P(E,\Theta)$ at the points (E_i,Θ_i) dictated by the method. The difference between the extracted $P(E_i,\Theta_i)$ and the known $P(E,\Theta)$ will tell us the accuracy of the method.

All of the integrals are computed using the integration limits listed in Table I by straightforward Hermite or Legendre quadrature. In all test cases, the number of integration points was increased until convergence was obtained for both the forward convolutions required to generate the $\{R_i\}$ as well as the integrals of Eqs. (4) and (15) which are need-

TABLE I. Experimental parameters.

Interaction volume coordinates		
$\|x\| < 0.15$ cm	$\|y\| < 0.15$ cm	$\|z\| < 0.15$ cm
Ionizer (detector) volume coordinates		
$\|X\| < 0.2$ cm	$\|Y\| < 0.2$ cm	$\|Z\| < 0.15$ cm
Nominal neutral particle flight path	$L_D = 21.0$ cm	
Distance of nozzle from interaction region	$X_N = 5.0$ cm	
Molecular beam velocity distribution parameters		
Flow speed	$v_0 = 5.6 \times 10^4$ cm/s	
Second moment	$\beta = 4.0 \times 10^{-8}$ (cm/s)$^{-2}$	
Time bin width	$2\,\mu$s	

ed for the orders of the method treated here. The molecular beam speed distribution was assumed to be a supersonic distribution which is described to a high degree of accuracy by

$$W(v) = N_v e^{-\gamma(v - v_0)^2}. \tag{19}$$

v_0 is the flow speed and γ is related to the second moment of the molecular beam velocity distribution. Of course, other molecular beam weighting functions $W(v)$ can be used with no modification to the method, except for choosing the appropriate quadrature scheme. In the examples that follow, unless otherwise specified, the translational energy distribution parameters are given in units consistent with the energy expressed in kilocalories.

A. Isotropic photodissociation

Consider the case of an isotropic, photofragmentation ($\beta = 0$) of a molecule into two fragments of masses 56 and 140 with a Boltzmann translational energy distribution of the form

$$P(E) = e^{-\zeta E}, \tag{20}$$

where ζ can be used to adjust the temperature of the translational energy distribution. Figure 2 shows the ideal experimental laboratory TOF data at several detector angles for both photofragments for the value $\zeta = 1/3$ kcal^{-1}. Figure 3 shows the difference between the extracted and the known $P(E)$ using the linear approximation of Eq. (9). The difference curves, one for each of the detector angles shown in Fig. 2, show that the translational energy distribution is determined with higher accuracy from the lighter mass TOF data. Since the lighter mass is scattered with larger center-of-mass velocities, all time bins will sample a smaller range of transla-
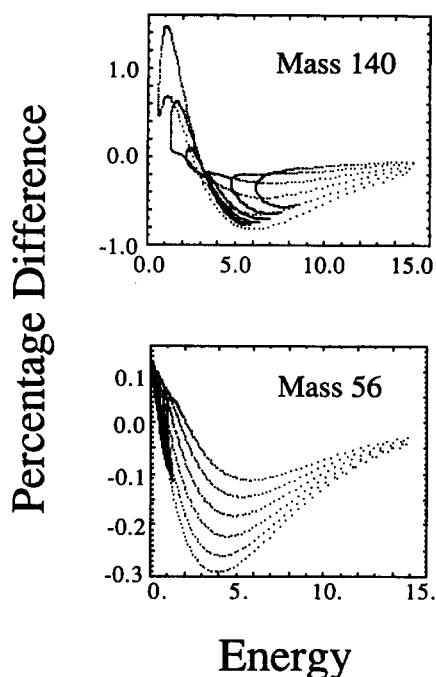

FIG. 3. Percentage difference between the known translational energy distribution of Eq. (20) for $\zeta = 1/3$ kcal^{-1} and the translational energy distribution extracted from the exact time-of-flight data using the linear approximation [Eq. (9)] for both photofragments.

tional energies for the lighter mass, thereby more accurately recovering the $P(E)$.

The double valuedness or looping back of each difference curve can be understood as follows. For a given detector angle, the average energy of each successive time bin, E_i, decreases until the center-of-mass and laboratory velocity vectors are perpendicular, after which E_i increases approaching an asymptotic energy which has the photoproducts traveling with a velocity which exactly cancels the initial molecular beam velocity. Hence, the TOF data at a fixed detector angle samples the $P(E)$ at nearly the same average energy for two well separated time bins over a finite energy range. Figure 4 shows the average energy and the dispersion in energy sampled by each bin for the heavier photofragment and illustrates the range of energy probed twice for a fixed detector angle. The double valuedness of the difference curves given in Fig. 3 (best seen in the heavier mass) is simply a result of the slightly different accuracies of the linear approximation for the pairs of time bins with nearly equal average energies.

As a second example consider a Gaussian translational energy distribution of the form

$$P(E) = e^{-\zeta(E - E_0)^2}, \tag{21}$$

where ζ can be used to adjust the width of the translational energy distribution and E_0 determines the peak position of the translational energy distribution. Figure 5 shows the ideal experimental laboratory TOF data at several detector angles for both masses for the parameter values $\zeta = 1/3$ kcal^{-2}, $E_0 = 5$ kcal. Figure 6 shows the difference between the extracted and known Gaussian $P(E)$ for the linear approximation of Eq. (9). For the Gaussian translational energy distribution the linear approximation is expected to be
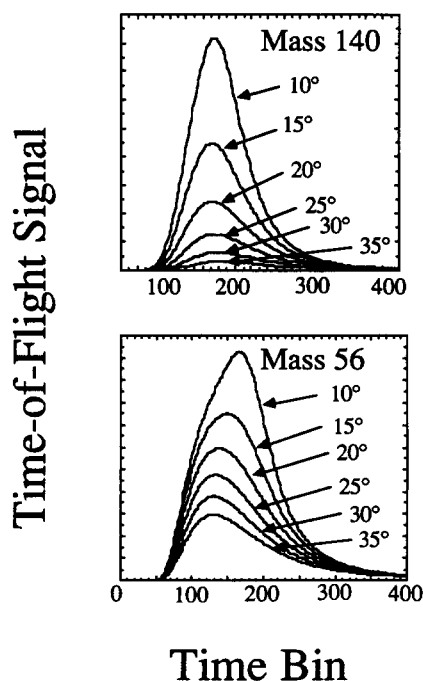

FIG. 2. Exact time-of-flight distributions for the two photofragment masses at the indicated laboratory detector angles for the Boltzmann translational energy distribution of Eq. (20) for $\zeta = 1/3$ kcal^{-1}.
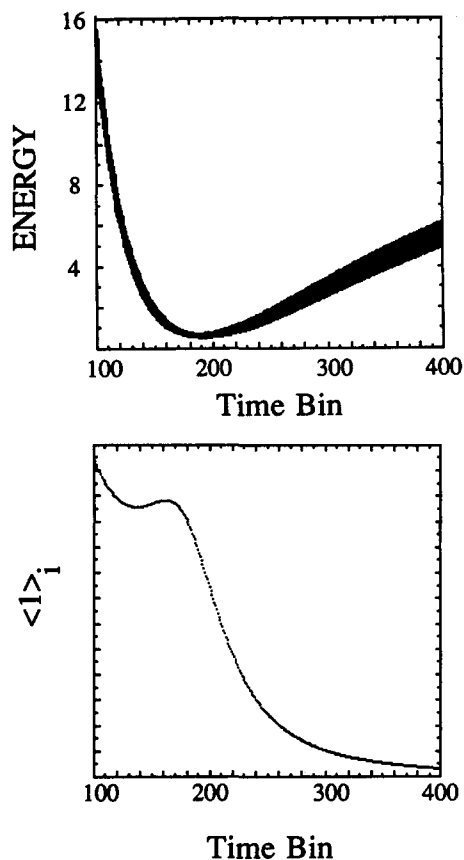
FIG. 4. The average center-of-mass energy and energy interval sampled (top) and the volume elements (bottom) for each time bin at a detector angle of 10° for the heavier photofragment.
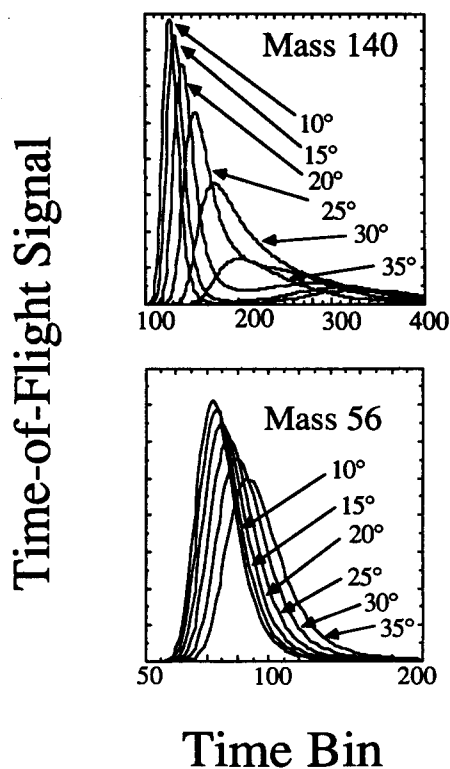

FIG. 5. Exact time-of-flight distributions for the two masses at the indicated laboratory detector angles for the Gaussian translational energy distribution of Eq. (21) for $\zeta = 1/3$ kcal^{-2} and $E_0 = 5$ kcal.

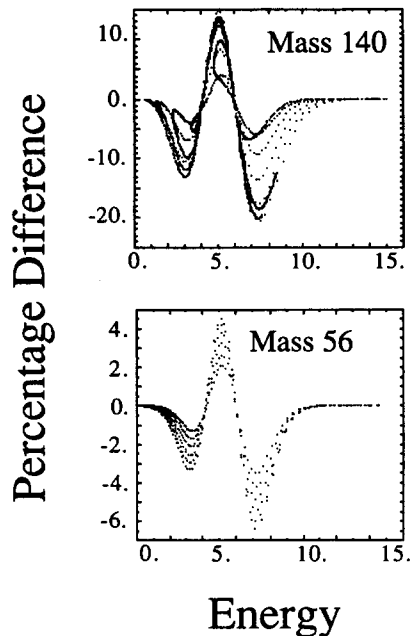FIG. 6. Percentage difference between the known translational energy distribution of Eq. (21) for $\zeta = 1/3$ kcal^{-2} and $E_0 = 5$ kcal and the translational energy distribution extracted from the time-of-flight data using the linear approximation [Eq. (9)] for both photofragments.

poorer because the Gaussian distribution changes rapidly and nonmonotonically over a small energy interval compared to the Boltzmann distribution. The locations of the largest deviations are clearly shown in Fig. 7 where the $P(E_i)$ extracted using the linear approximation are directly compared to the known Gaussian $P(E)$. The largest deviations occur where the second derivative of the Gaussian
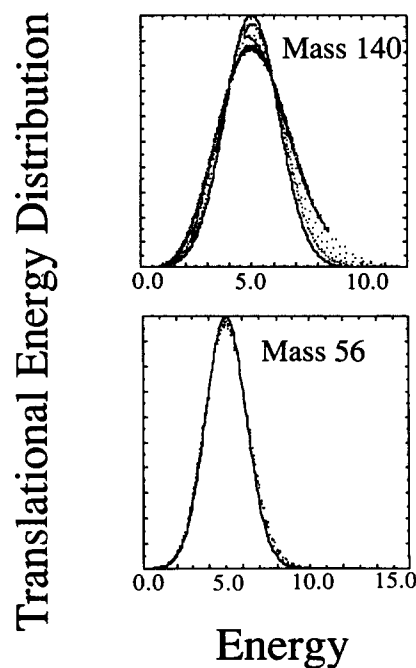

FIG. 7. A comparison of the extracted translational energy distribution using the linear approximation (points) and the known Gaussian translational energy distribution (solid line) of Eq. (21) for $\zeta = 1/3$ kcal^{-2} and $E_0 = 5$ kcal.

$P(E)$ is large. The magnitude of the error depends on the experimental averaging and can be understood when the correction terms arising form the derivatives of the translational energy function are taken into account. This is explored in Sec. III C below.

As a second test we used the same $\{R_i\}$ as above but added a random error component which mimics a large constant background count rate in the detector for each detector angle setting as is typically present in most experiments. Figures 8, 9, 10, and 11 show the extracted $P(E)$ for both the Boltzmann and Gaussian model $P(E)$ functions of Eqs. (20) and (21) for the lighter and heavier masses using all of the time bins whose average energy E_i is less than 15 kcal. The large scatter in the extracted $P(E)$ at certain energies is caused by using the points in the TOF distributions at very long times. These points represent scattering which produce products which are moving more and more slowly in the laboratory frame. Eventually, the products detected in these time bins are characterized by a center-of-mass recoil velocity which exactly cancels the initial molecular beam velocity.

The scatter in the extracted $P(E)$ for the long time TOF data points can be understood by referring to Eq. (9). The volume elements $\langle 1 \rangle_i$ become arbitrarily small at sufficiently long times because the Jacobian factor [see Eq. (A6)] is proportional to the square of the laboratory velocity. An example of how the volume elements vary with bin is shown in Fig. 4. The noise in the data is divided by smaller and smaller volume elements to determine the $P(E)$ resulting in an arbitrarily large scatter in the extracted translational energy distribution if sufficiently delayed channels are invert-
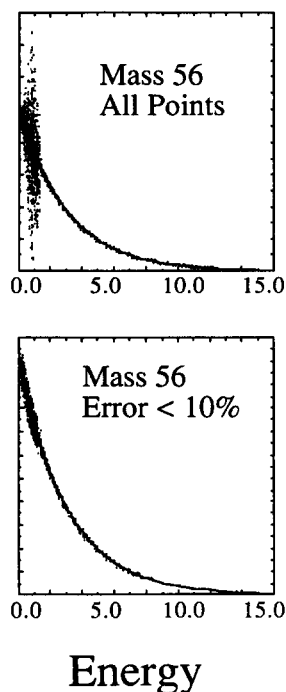

FIG. 9. The extracted (points) and model translational energy distribution (solid line) for the Boltzmann translational energy distribution of Eq. (20) using TOF data with $\pm 3\%$ noise for the mass 140 photofragment. The upper panel shows the extracted points for all TOF channels with an average energy less than 15 kcal, while the lower panel shows only those points with relative error less than 10%.

FIG. 8. The extracted (points) and model translational energy distribution (solid line) for the Boltzmann translational energy distribution of Eq. (20) using TOF data with $\pm 3\%$ noise for the mass 56 photofragment. The upper panel shows the extracted points for all TOF channels with an average energy less than 15 kcal, while the lower panel shows only those points with relative error less than 10%.
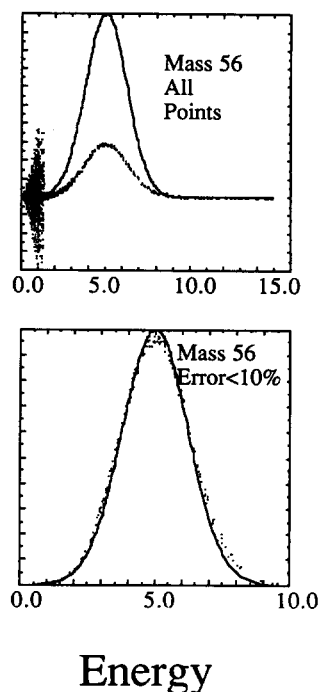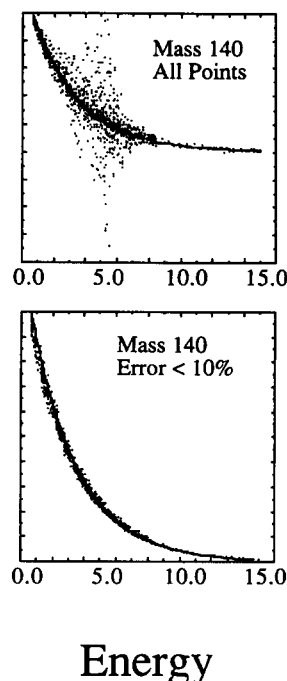

FIG. 10. The extracted (points) and model translational energy distribution (solid line) for the Gaussian translational energy distribution of Eq. (21) using TOF data with $\pm 3\%$ noise for the mass 56 photofragment. The upper panel shows the extracted points for all TOF channels with an average energy less than 15 kcal, while the lower panel shows only those points with relative error less than 10%.
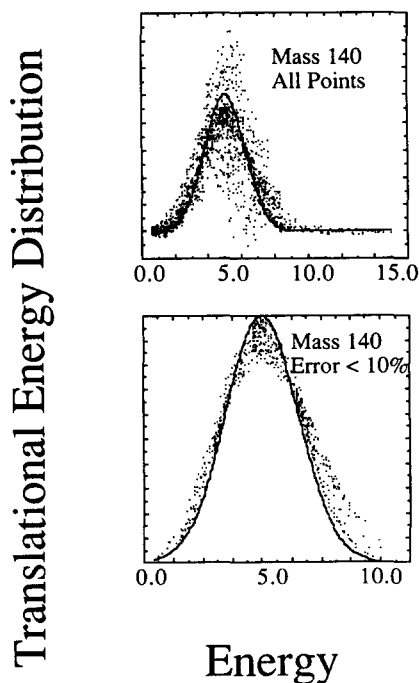
FIG. 11. The extracted (points) and model translational energy distribution (solid line) for the Gaussian translational energy distribution of Eq. (21) using TOF data with $\pm 3\%$ noise for the mass 140 photofragment. The upper panel shows the extracted points for all TOF channels with an average energy less than 15 kcal, while the lower panel shows only those points with relative error less than 10%.
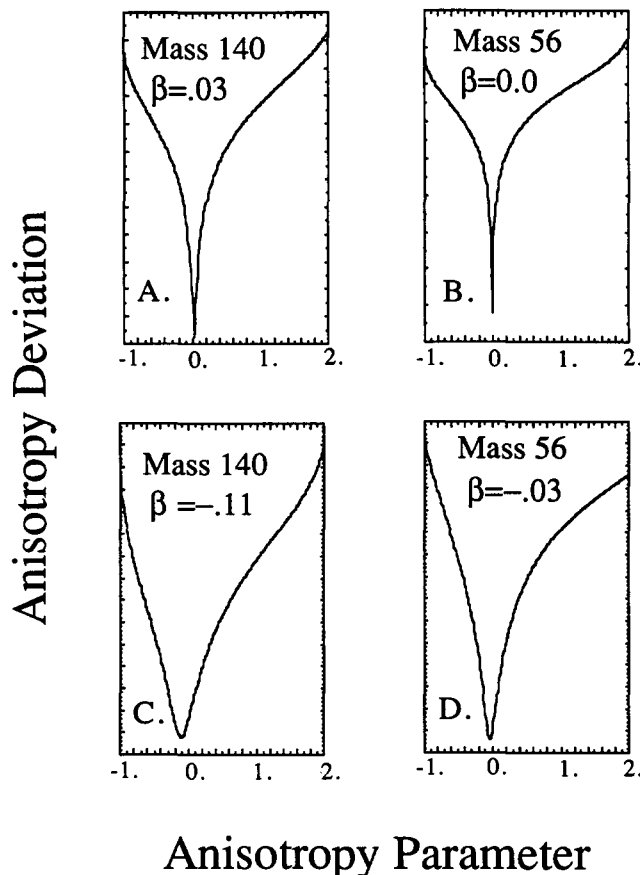

Anisotropy Parameter

FIG. 12. The anisotropy parameter error function, Eq. (16), for the Boltzmann translational energy distribution for both product masses without noise [(a) and (b)] and with noise [(c) and (d)] in the TOF data.

ed. However, if we display only the $P(E)$ points with relative error of less than 10%, then we are left with the results shown in the lower panels of Figs. 8, 9, 10, and 11. For lack of a better term, we call this selection of a subset of the $P(E)$ points based on their relative error as *filtering*. Filtering the $P(E)$ points allows one to analyze all of the experimental TOF data without any restriction. Data points are rejected at the end of the analysis based solely on their associated error.

B. Anisotropic photodissociation

In Fig. 12 we have plotted $B(\beta)$ as defined in Eq. (16) for the Boltzmann translational energy distribution for both masses using the exact and noisy TOF data. The results for the Gaussian translational energy distribution are similar and are not shown. For noisy TOF data, the $B(\beta)$ curve can be severely distorted unless one uses only the $P(E_i)$ points with relative error less than $\sim 10\%$ to compute $B(\beta)$. The effect of noise is to smooth out the sharp cusp of the $B(\beta)$ function. The computed values for β are near the correct value of $\beta = 0$ although the presence of noise in the TOF data induces a small anisotropy. We have calculated $B(\beta)$

using TOF data generated by other values of β (including the endpoints $- 1,2$) for both translational energy distributions with similar results to the particular example shown here.

If β is energy dependent, the procedure defined here can be followed by considering only data points within limited energy intervals. Of course, one can also perform the experiments by rotating the laser polarization vector leaving the mass spectrometer angle fixed, and measure directly the polarization anisotropy for each time bin.

C. Quadratic approximation

To illustrate the complications induced by inclusion of the second derivative term in Eq. (17), the second derivatives are approximated by discrete differences using the adjacent R_{i-1}, R_{i+1}:

$$\frac{P''(E_i)}{2} \approx \frac{(E_{i+1} - E_i)(R_{i-1}/\langle 1 \rangle_{i-1}) + (E_{i-1} - E_{i+1})(R_i/\langle 1 \rangle_i) + (E_i - E_{i-1})/(R_{i+1}/\langle 1 \rangle_{i+1})}{D}, \qquad (22)$$

where

$$D = E_{i-1}^2 (E_{i+1} - E_i)$$
$$+ E_i^2(E_{i-1} - E_{i+1}) + E_{i+1}^2 (E_i - E_{i-1}). \qquad (23)$$

Hence we can write

$$P(E_i) \approx \frac{R_i}{\langle 1 \rangle_i} - [E_i^2 - (E_i)^2] \frac{P''(E_i)}{2}, \qquad (24)$$

where $P''(E_i)/2$ is understood to be evaluated by Eq. (22).

To show how the derivative correction terms can improve the fit to the data, Fig. 13 shows the difference curve for the exact TOFs of the Gaussian translational energy distribution using the second derivative correction term [Eq. (22)]. For the lighter mass, the error has been reduced by a factor of 5 while for the heavier mass, the error has been decreased by a factor of 2 at best. The heavier mass shows a large residual scatter because the dispersion in energy [$E_i^2 - (E_i)^2 \approx 1.5$ kcal^2 for the modeled experimental conditions] is significant so the neglected third and higher order derivative terms in the Taylor series expansion are required to accurately recover the translational energy function from the heavier mass TOF data. The dispersion in energy is large because the modeled experimental apparatus has a 5% velocity resolution and an initial 10% dispersion of molecular beam speeds.

It is possible to define alternative formulas for the second derivative required in the quadratic approximation. For example, the second derivatives can be defined using the adjacent (but unknown) $P(E_i)$. In this case, a set of tridiagonal, coupled linear equations can be easily solved for the $P(E_i)$. However, the solution to the tridiagonal equations always has an oscillatory structure which cannot be removed by the imposition of boundary conditions. This oscillatory structure is inherent because the equations are stiff, second-order differential equations with one of the homogeneous solutions varying much more rapidly than the grid spacing given by the $\{E_i\}$. The easiest method to remove the oscillations would be to use a denser grid of energy points so the contribution of the rapidly varying homogeneous solution
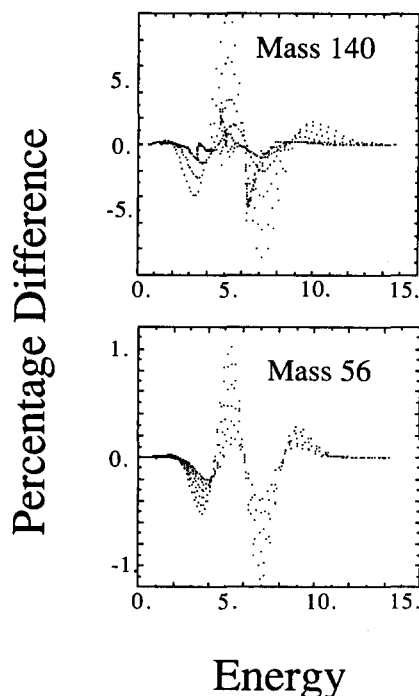

FIG. 13. The extracted (points) and model translational energy distribution (solid line) for the Gaussian translational energy distribution of Eq. (21) using exact TOF data for both fragments including the quadratic correction of Eq. (22).

does not grow. In the method of moments approach, the grid is fixed at $\{E_i\}$ so this straightforward cure is not possible. The approximation to the second derivatives given by Eq. (22) decouples the tridiagonal equations and removes the oscillatory structure.

When the quadratic approximation using the second derivative correction term of Eq. (22) is applied to data with statistical noise, poor results are obtained. To see why the second derivative correction is sensitive to small noise levels, assume that the first and second moments can be locally approximated by

$$E_i - E_{i-1} \sim E_{i+1} - E_i = \delta, \qquad (25)$$

$$E_{i+1}^2 \approx E_i^2 + \frac{dE_i^2}{dE_i}\delta + \frac{1}{2}\frac{d^2E_i^2}{dE_i^2}\delta^2 + \cdots, \qquad (26)$$

$$E_{i-1}^2 \approx E_i^2 - \frac{dE_i^2}{dE_i}\delta + \frac{1}{2}\frac{d^2E_i^2}{dE_i^2}\delta^2 + \cdots. \qquad (27)$$

Using these approximations, the denominator of the second derivative correction term is

$$D = E_{i-1}^2(E_{i+1} - E_i) + E_i^2(E_{i-1} - E_{i+1})$$
$$+ E_{i+1}^2(E_i - E_{i-1})$$
$$\approx \frac{d^2E_i^2}{dE_i^2}\delta^3. \qquad (28)$$

Since both the random error component of the $\{R_i\}$ and the volume elements $\langle 1 \rangle_i$ are approximately equal in magnitude for nearby bins, then using the same approximations of Eqs. (25)–(27) in the worst case the numerator of the second derivative of Eq. (19) is

$$\left| (E_{i+1} - E_i)\frac{\Delta R_{i-1}}{\langle 1 \rangle_{i-1}} \right| + \left| (E_{i-1} - E_{i+1})\frac{\Delta R_i}{\langle 1 \rangle_i} \right|$$
$$+ \left| (E_i - E_{i-1})\frac{\Delta R_{i+1}}{\langle 1 \rangle_{i+1}} \right| \approx \frac{4\delta\Delta R_i}{\langle 1 \rangle_i}. \qquad (29)$$

Combining Eqs. (25)–(29), the error in the translational distribution from the second derivative correction near the peak of the Gaussian distribution where $\delta \approx 0.2$ kcal, $E_i \approx 5$ kcal, $[(E_i^2 - (E_i)^2] \approx 1.5$ kcal^2, and $d^2E_i^2/dE_i^2 \approx 20$ is

$$\Delta P(E_i) \approx \frac{[E_i^2 - (E_i)^2](4\delta\Delta R_i/\langle 1 \rangle_i)}{(d^2E_i^2/dE_i^2)\delta^3} \approx \frac{10\Delta R_i}{\langle 1 \rangle_i} \qquad (30)$$

which is ten times larger than the error of the linear correction. It we wanted a 1% error in the second correction, the statistical error in the data would have to be less than 1/1000 which is impractical to obtain experimentally.

The poor handling of noise by Eq. (22) results because the error in the data is not considered when calculating the second derivatives. The random fluctuations for adjacent bins can appear as an enormous second derivative using Eq. (22). We have found that a least-squares cubic spline fitting technique[4] that takes into account the errors in the data and minimizes the second derivative produces a smooth fit through the data with an error magnification of one. Using this least-squares method to compute the second derivative correction, the translational energy distribution is recovered with the same noise sensitivity as the linear approximation.

IV. CONCLUSION

We have demonstrated a method for extracting the center-of-mass DFCS (as measured in a crossed laser-molecular beam experiment) for a binary photofragmentation that makes no prior assumption about the shape of the translational energy distribution. The method has the following advantages:

(1) The $P(E)$ function is determined at points $\{E_i\}$ that are probed by the data in an unbiased manner.

(2) The method provides a natural hierarchy for analyzing experiments of progressively higher resolution which converges if the experimental resolution warrants such higher order treatment.

(3) The method correctly propagates the experimental error in the TOF distributions to the error in the value of the experimentally determined $P(E_i)$ at each E_i, showing where the function $P(E)$ is best determined by the data.

In a future paper will will apply the method to reactive scattering.

ACKNOWLEDGMENTS

APPENDIX

In this Appendix, explicit expressions for the integrand in terms of the integration variables are derived. Let $r = (x,y,z)$ label the point in the interaction region where the photodissociation occurs. We assume that the interaction region is centered at the origin of the space fixed coordinate system. Let $R = (X,Y,Z)$ label the point relative to the center of the ionizer where the photofragment is ionized or detected. If L_D is the distance between the center of the ionizer and the center of the interaction region and Ω_{lab} is the angle the detector has been rotated from the molecular beam axis, then

$$\mathbf{R} = [(L_D + X)\cos \Omega_{lab} - Y \sin \Omega_{lab},$$
$$(L_D + X)\sin \Omega_{lab} + Y \cos \Omega_{lab}, Z] . \tag{A1}$$

The molecular beam is assumed to issue from a point source located at $(-x_N, 0, 0)$. The molecular beam velocity vector at a point (x,y,z) in the interaction region is

$$\mathbf{v} = \frac{v(x_N + x, y, z)}{\sqrt{[(x_N + x)^2 + y^2 + z^2]}} . \tag{A2}$$

Using these definitions, the laboratory velocity of a photofragment dissociated at position r, detected a later time t at location R is

$$\mathbf{v}_{lab} = \frac{(\mathbf{R} - \mathbf{r})}{t} . \tag{A3}$$

The center-of-mass velocity of this same photofragment is

$$\mathbf{u}_{c.m.} = \mathbf{v}_{lab} - \mathbf{v} . \tag{A4}$$

Since we desire the DFCS with respect to solid angle and energy in the center-of-mass coordinates, we have to relate the DFCS measured in the laboratory frame (laboratory speed and laboratory solid angle) to the one appropriate for the center-of-mass frame. We refer to Ref. 3 for the details and here we give the final result for the Jacobian for a continuous center-of-mass energy distribution for a binary photodissociation:

$$\frac{d^2\sigma}{d\Omega_{lab}\, dv_{lab}} = \left(\frac{v_{lab}}{u_{c.m.}}\right)^2 \left(\frac{m^2 u_{c.m.}}{\mu}\right) \frac{d^2\sigma}{d\Omega_{c.m.}\, dE_{c.m.}} . \tag{A5}$$

μ is the reduced mass of the binary photofragments and m is the mass of the detected photofragment. For an inefficient ionizer, the ionization probability is proportional to the time the particle spends in the ionization region and therefore is weighted by $1/v_{lab}$. When this detection efficiency factor is incorporated in the Jacobian in Eq. (A5) above, and the expression converted to the independent variables (v_{lab}, t) the new Jacobian factor becomes

$$J(t, \mathbf{r}, \mathbf{R}, v) = \left[\left(\frac{v_{lab}^2}{u_{c.m.}}\right)\left(\frac{m^2}{\mu}\right)\right] t . \tag{A6}$$

Finally,

$$E = (m u_{c.m.})^2 / 2\mu \tag{A7}$$

and

$$\cos \Theta = \frac{(\mathbf{u}_{c.m.} \cdot \mathbf{e})}{u_{c.m.}} , \tag{A8}$$

where e is a unit vector in the direction of the laser polarization.

[1] S. C. Yang and R. Bershohn, J. Chem. Phys. 61, 4400 (1974), and references cited therein.
[2] R. von Mises, *Mathematical Theory of Probability and Statistics* (Academic, New York, 1964), p. 384.
[3] G. L. Cachen, J. Husain, and R. N. Zare, J. Chem. Phys. 69, 1737 (1978).
[4] C. A. Reinsch, Numerishe Mathematik 10, 177 (1967).